Dissociation of vibronic states of C–$^1A'$ DCN: Quantum treatment

David T. Chuljian, Judy Ozment, and Jack Simons

Department of Chemistry, University of Utah, Salt Lake City, Utah 84112
(Received 20 June 1983; accepted 14 September 1983)

The rates of dissociation of several vibrational states of $n\pi^*$ excited (C–$^1A'$) DCN have been determined via quantum dynamical means in which only the CD stretching and DCN bending motions are treated. The *ab initio* configuration interaction potential energy surface used in our earlier classical trajectory study of these same dissociation rates was employed in the present study. The results of this quantal study tend to support our earlier prediction that $v_2 \rightarrow v_1$ (bending-to-stretching) energy transfer plays an important role in determining the dissociation rates of these vibronic states. Surprisingly, the absolute rates obtained via the quantum method are in quite close agreement with a certain component of the classically determined rates.

I. INTRODUCTION

The low lying electronic states of HCN and DCN, in particular the singlet states of A' symmetry, have been investigated by Herzberg[1] and others,[2] more recently by MacPherson and Simons[3] (hereafter referred to as MS). The B and C states have been identified as $^1A'$ (the molecule has a bent equilibrium position in both states) and lie about 6.8 and 8.2 eV above the ground state $X(^1\Sigma^+)$. The C state is especially interesting in that it dissociates to a ^2S H atom and an excited $(X\,^2\Sigma^+)$ CN radical. The latter, upon returning to its ground state, emits fluorescence as a result of which the production of CN from photodissociated HCN or DCN molecules can be monitored.

The recent experiments of MS, in addition to measuring the absorption spectrum ($X \rightarrow C$) for HCN and DCN, also included measurements of the photofragment excitation spectrum (PFES) and the polarization of the CN fluorescence. The PFES, as indicated above, monitors the dissociation of the metastable molecules as a function of exciting wavelength, i.e., as various vibrational levels of the C state are populated. The absorption linewidths give information about the lifetimes of the various vibrational states. The fluorescence polarization measurements indicate whether the metastable states decay on a time scale that is short or long with respect to the rotational period of the molecule (low polarization retention indicates a relatively long-lived vibronic state).

MS assigned[3] vibrational quantum numbers to the peaks in the PFES of HCN and DCN. The v_1 mode is the NC--H stretch, while v_2 corresponds to a bending of the molecule. The HC--N stretching quantum number v_3 is ignored both in our earlier classical dynamics study and in our quantum analysis because we are attempting to investigate only those spectral features for which the v_3 mode remains in its ground state.[4] This allows us to consider a two-dimensional potential energy surface in which the CN bond is passive. MS concluded that the C state of HCN supports a v_2 (bending) progression only for a stretching quantum number (v_1) of zero; for $v_1 > 0$, no v_2 progression was observed, although a contribution from an underlying continuum was inferred, implying that HCN dissociates extremely rapidly if the NC--H stretch is excited. For DCN, v_2 progressions were observed for $v_1 = 0$, 1; also a v_2 series for $v_1 = 2$ was inferred[3] on the basis of unusual intensity patterns in the spectrum. For both isotopes, the fluorescence polarization retention generally decreased as the wavelength of the exciting light increased, although the decrease was not monotonic.

MS interpreted their spectrum as indicating the presence of two dissociation mechanisms for HCN. The first was assumed active for $v_1 = 0$ HCN ($v_1 = 0$, 1, 2 for DCN), but with further excitation of the stretching mode, a "competing mechanism" increased in rate and led to rapid dissociation of the molecule. MS did not describe the competing mechanism, nor why it is apparently operative for $v_1 = 1$ HCN (which has *less* NC--H stretching energy than $v_1 = 2$ DCN, for which the competing mechanism is *not* operative).

Our first efforts[5] at interpreting the MS experimental data were directed at obtaining a good quality configuration interaction (CI) description of the HCN energy surfaces for the B and C states. These CI calculations were carried out for a wide variety of geometries (at fixed C--N bond length) and the resultant electronic energies were interpolated by using the method[6] of Downing *et al.* Examination of this global energy surface (see Fig. 1) led us to conclude that a tunneling mechanism could adequately explain all the data. Examination of Fig. 1 shows that no barrier to dissociation exists for angles near the equilibrium configuration (157°), but for distorted molecular geometries ($\theta > 164°$ or $\theta < 140°$), a barrier suitable for tunneling exists. We hypothesized[5] that for low v_1 (0 for HCN, 0, 1, 2 for DCN) only when the molecule contains sufficient bending (v_2) energy does it sample regions of the energy surface at which predissociation can take place, via tunneling through the barrier; as v_1 is increased, the H (or D) atom possesses sufficient energy to *directly* escape the potential well thus leading to continuum behavior. A simple model, based on separable harmonic oscillator modes for v_1 and v_2 and crude tunneling estimates, lent support to this hypothesis. In summary, the model[5] predicted the general trends (onset of predissociation as v_2 increases and switch to continuum behavior as v_1 increases) very well, except that it predicted no v_2 progression for $v_1 = 2$ for DCN. As the experimental as-

 0021-9606/84/010176-10$02.10

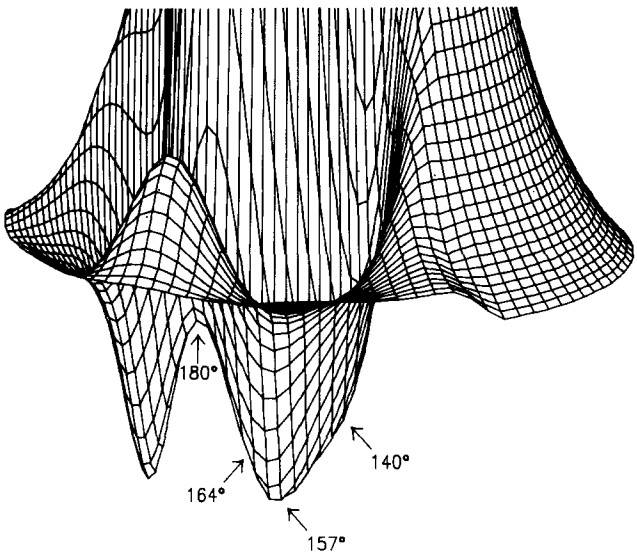

FIG. 1. The *ab initio* potential energy surface for C-state HCN or DCN. The energy (vertical scale) ranges from -96.600 to -92.645 hartrees. The C and N atoms are held fixed, so the energy is a function only of the position of the H atom. The HCN equilibrium bond angle occurs at $\theta = 157°$ and there is a saddle point at $\theta = 180°$. A radial barrier to dissociation begins to appear at $\theta > 164°$ and $\theta < 140°$.

signment of that series was somewhat tentative, the disagreement was not considered a major failure of the model.

We next performed classical trajectory calculations[7] on distributions of initial coordinates and momenta which mimicked the various (v_1, v_2) states of DCN, utilizing a polynomial fit of the same C state CI energy surface (again, fixing the length of the C--N bond). To determine initial momenta appropriate to each of the v_1, v_2 states, we used the MS experimental energy spacings for all v_2 values and for $v_1 = 0, 1$, and we used a harmonic extrapolation of the same for $v_1 = 2, 3$. MS did not report anharmonicity in v_1, so unambiguous assignment of their results was restricted to $v_1 = 0, 1$. These dynamical simulations included approximate tunneling rate estimates. The results of our classical study indicated that tunneling is *not* important in the predissociation mechanism, but that $v_2 \rightarrow v_1$ energy transfer leads to the H (or D) atom's classical escape. We saw that increasing the excitation in the v_1 mode caused an increase in the rate of fragmentation. Once again, the correct trends (onset of predissociation and switch to purely dissociative behavior) were reproduced.

Although these earlier classical investigations were quite successful, we had one important motivation to carry out the quantum dynamical study of DCN described here. A quantum study on this same potential energy surface would allow a direct comparison of the results of quantum and classical studies of such unstable molecules. Considerable work has been done using classical mechanics on molecular scale systems, but the ability of such studies to simulate the true quantum behavior of such systems should be questioned. Such a direct comparison as this, on a problem closely approximating a real molecular system, therefore provides insight as to how one should interpret classical results on quantum systems (see Sec. V).

We turn first to a discussion of the quantum mechanical methods used in our study (Sec. II) and of the specific potential energy surface and vibrational basis sets (Sec. III). Then, in Sec. IV, we will analyze our results and make comparisons with those of our earlier classical mechanical work.

II. REVIEW OF THE COORDINATE ROTATION METHOD

The coordinate rotation (CR) or complex coordinate method[8] has proven useful in determining state energies and lifetimes of autoionizing atoms, molecules, and anions. More recently, its use has been extended to metastable heavy particle systems by Chu,[9(a)] Christoffel and Bowman,[9(b)] Hedges and Reinhardt,[9(c)] and Bacic *et al.*[10] The underlying foundations of the CR method as well as its connections with such scattering techniques as the Siegert method[11] are treated in numerous places[8,12] in the literature. Here we simply review[13] how the CR method is implemented for systems involving distinguishable heavy particles such as DCN.

The Hamiltonian H describing the motion of the DCN nuclei on the C-state potential energy surface involves kinetic energy along three internal coordinates and three orientational angles. One of these coordinates (the radial distance r of the D atom to the center of mass of the CN moiety) is singled out for special attention because it is the coordinate which asymptotically describes relative translation of the D + CN fragments. The CN bond-length coordinate and all orientational and bond-angle coordinates remain intact in the DCN $\rightarrow$ D + CN event; only r undergoes a qualitative change from quasi-bound vibration-like motion to unbound translational motion.

For energies which lie above the dissociation threshold of C-state DCN, the various v_1, v_2 levels being studied here are not bound states; they are only metastable. For this reason, conventional basis-set diagonalization of H cannot straightforwardly be used to locate their energies or compute their widths; the Ritz variational principle is not useful for states which lie in the continuum. Use of the CR method allows one to extract from the (complex) eigenvalues[8] $E_r - i\Gamma/2$ of the so-called complex scaled Hamiltonian $H(\eta)$ the energies E_r and lifetimes $\tau = \hbar/\Gamma$ of the metastable states. Construction of the rotated Hamiltonian $H(\eta)$ is carried out by replacing the asymptotic radial coordinate r discussed above by ηr everywhere r appears in H. The complex scale parameter η has magnitude α and phase θ: $\eta = \alpha \exp(i\theta)$. Because r appears in the kinetic energy as r^{-2}, the complex scaled kinetic energy is simply η^{-2} times the unscaled kinetic energy. Scaling the r dependence of the potential energy V in H is more difficult because V is not a simple homogeneous function of r. The scaling of $V(r)$ in the particular case at hand is treated in Sec. III E.

Given that the operator $H(\eta)$ can be constructed, the

CR method instructs us to form the matrix representative of $H(\eta)$ in a basis and then to find the (complex) eigenvalues $E_k(\eta)$ of this matrix. By following each of these eigenvalues as α and θ are varied, one attempts to identify those eigenvalues which display stability (i.e., small sensitivity to changes in α or θ) over some range of α and θ values. This searching is often accomplished by plotting the eigenvalues as functions of θ for fixed α. Such a graph is called a θ-trajectory. According to the CR theory,[8] a resonance state's complex energy should vary with θ until θ exceeds some critical value θ_c, beyond which the energy should be unchanged as θ further varies. In practice, one usually experiences a considerable reduction in the θ dependence of E_k once $\theta > \theta_c$, but perfect θ independence is hardly ever seen.

With this brief overview of the CR method in hand, let us now move on to explore its implementation in the DCN predissociation under study in this work.

III. DESCRIPTION OF THE PRESENT STUDY

A. Definition of the problem

In this study, a fixed DC--N bond length (1.300 Å) was employed for computational tractability as well as to allow comparison with our earlier classical studies.[7] The existence of the CN--D isomer's potential well was essentially ignored because C state DCN is known[14] to not isomerize appreciably to CND. At the total energies which we consider, the DCN cannot access the CND region, and thus our use of a surface which ignores (by being quite repulsive) the CND geometry is justified.

All of our calculations were designed to locate metastable states (resonances) with energies less than ~ 1100 cm^{-1} above the dissociation threshold. Our classical trajectory calculations had indicated[7] that, even in this energy range, states with long, medium, and short lifetimes should be found. Thus, our aspirations were not to generate quantal energies and lifetimes for all 30 vibrational states which we examined classically; we were attempting to compare quantum and classical predictions only for a selected subset of these states. At energies well above 1100 cm^{-1}, the density of states becomes so high that the identification (i.e., labeling with v_1 and v_2 quantum numbers) of resonance states is much more difficult.

B. Form of the potential energy surface

In order to utilize angular momentum coupling to simplify the quantal computation arising in this problem, we decided to fit our C-state potential surface to the following functional form[10,13]:

$$V(r,\theta) = \sum_{L=0}^{L_{\max}} V_L(r) P_L[\cos(\theta)] , \tag{1}$$

where P_l is the lth order Legendre polynomial. This potential energy function was constructed in three steps: (a) the energy of HCN was calculated by configuration interaction[5]; (b) the 150 different CI energies were fit to a polynomial expression $V(r,\theta)$ in r and $\cos(\theta)$, within an accuracy (average deviation of input points from the interpolated function) of about 50 cm^{-1}; and (c) for numerous values of r, the coordinate which represents the distance from the center of mass of the CN moiety to the H or D atom, numerical values of the $V_L(r)$'s of Eq. (1) were calculated by numerically projecting out the various $P_L[\cos(\theta)]$ components of the above polynomial expression for $V(r,\theta)$.

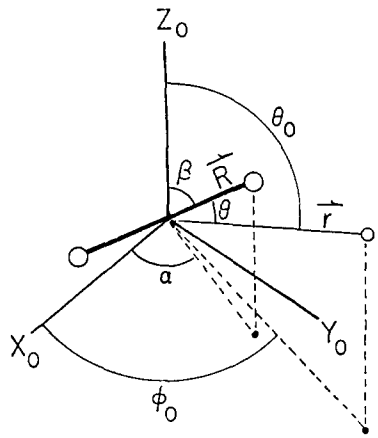

FIG. 2. The lab-fixed coordinate system used in this work.

The final compromise ($L_{\max} = 4$ or 5) between accuracy of the potential (compared to the polynomial expression for E) and computational expense (too many L values) was arrived at after much trial and error. The final $V_L P_L$ potential of Eq. (1) is about 400 cm^{-1} too deep at its minimum relative to the $V(r,\theta)$ potential used in our earlier classical trajectory calculations. This deviation should be kept in mind since it might influence our quantum/classical comparison given in Sec. V. However, viewing plots of the two energy surfaces shows that the shapes of the polynomial and $V_L P_L$ potentials are sufficiently similar that we feel this should not cause qualitative changes in the predicted energies and lifetimes. Further, as we show later, the bound-state energies obtained in our quantum calculations on the $V_L P_L$ surface are in reasonable agreement with the experimental results[3] of MS (see Sec. V A).

C. Dynamical equations

The coordinate system which we use to describe the motion of DCN is illustrated in Fig. (2). The six-dimension Hamiltonian of the system is

$$H = \frac{\hbar^2}{2\mu_{D,CN}} \nabla_r^2 + V(r,\theta) + \frac{j^2}{2\mu_{CN} R^2} , \tag{2}$$

where $\mu_{D,CN}$ is the reduced mass of D relative to the CN diatom, and V is the atom–diatom interaction potential of Eq. (1). The CN rotational kinetic energy involves the CN angular momentum j, the HC–N bond length R, and reduced mass μ_{CN}. There is no ϕ dependence in V because of the axial symmetry of the problem. We now proceed as in Ref. 10 to introduce eigenfunctions of the total angular momentum J^2 and J_z:

$$\psi_{jl}^{JM} = \sum_m \langle l, M-m; j, m | J, M \rangle \times Y_{j,m}(\beta,\alpha)\, Y_{l,M-m}(\theta_0, \phi_0) . \tag{3}$$

These eigenfunctions can be used as basis functions in

terms of which to expand the eigenstates of H corresponding to a fixed value of J, M as

$$\Psi_{JM}(\beta, \alpha, r, \theta_0, \phi_0) = \sum_{ij} \psi_{jl}^{JM} \phi_{jl}^{JM}(r) , \tag{4}$$

where the $\phi_{jl}^{JM}(r)$ describe the radial motion of H (D) relative to the CN. Substitution into $(H-E)\,\Psi = 0$, followed by the usual premultiplication and integration, gives coupled differential equations for the ϕ_{jl}^{JM}:

$$\delta_{l'l}\delta_{j'j}\left[-\frac{\hbar^2}{2\mu_{D,CN}}\left(\frac{1}{r^2}\frac{d}{dr}\left(r^2\frac{d}{dr}\right)-\frac{l(l+1)}{r^2}+\epsilon_j-E\right)\right]\phi_{jl}^{JM} + \sum_{jl}\langle\psi_{j'l'}^{JM}|\,V(r,\theta)\,|\psi_{jl}^{JM}\rangle\,\phi_{jl}^{JM} = 0 , \tag{5}$$

where ϵ_j is the rotational energy of the CN fragment. Notice that the $V(r, \theta)$ in Eq. (1) is expressed in terms of molecule-fixed coordinates r and θ, but the integration is over the lab-fixed angles α, β, θ_0, ϕ_0 of the ϕ_{jl}^{JM}. By the introduction of rotation matrices and the use of standard identities, the above V matrix element can be expressed as:

$$V_{j'l',jl}^{JM} = (-1)^{j+j'-l-l'}(2j+1)^{1/2}(2j'+1)^{1/2} \times\sum_{\mu}\begin{pmatrix} j' & l' & J \\ 0 & \mu & -\mu\end{pmatrix}\begin{pmatrix} j & l & J \\ 0 & \mu & -\mu\end{pmatrix}\int Y_{l',\mu}^{*}(\theta,\phi) \times V(r,\theta)\,Y_{l,\mu}(\theta,\phi)\sin(\theta)d\theta\,d\phi , \tag{6}$$

where the $\left(\begin{smallmatrix} j & l & J \\ 0 & \mu & -\mu\end{smallmatrix}\right)$ are the well known 3-j symbols[15] of angular momentum coupling theory. We can now take advantage of the form of V [see Eq. (1)] to separate the radial and angular part of the integration in Eq. (6). After additional use of standard identities involving integrals of products of three spherical harmonics, we arrive finally at

$$V_{j'l',jl}^{JM} = \sum_{L=0}^{L_{max}} f_L(jl,j'l',J)V_L(r) , \tag{7}$$

where the f_L are the well-known Percival–Seaton coefficients[16]

$$f_L(jl,j'l',J) = (-1)^{j+j'-l-l'}[j]^{1/2}[j']^{1/2}[l]^{1/2}[l']^{1/2} \times\sum_{L}\sum_{\mu}\begin{pmatrix} j' & l' & J \\ 0 & \mu & -\mu\end{pmatrix}\begin{pmatrix} j & l & J \\ 0 & \mu & -\mu\end{pmatrix} \times(-1)^{\mu}\begin{pmatrix} l & i' & L \\ 0 & 0 & 0\end{pmatrix}\begin{pmatrix} l & l' & L \\ \mu & -\mu & 0\end{pmatrix} \tag{8}$$

and $[j] = 2j+1$.

We now restrict our consideration to the case $J = M = 0$. The justification for this restriction is the observed lack of significant J dependence[7] in the decay kinetics obtained in our classical trajectory calculations (in which various values of J were explored). For this $J = 0$ case, Eq. (5) reads

$$\delta_{l'l}\left[-\frac{\hbar^2}{2\mu_{D,CN}}\left[\frac{1}{r^2}\frac{d}{dr}\left(r^2\frac{d}{dr}\right)-\frac{l(l+1)}{r^2}\right]+\epsilon_l-E\right]\phi_l(r) + \sum_{l}\sum_{L} f_L(ll,l'l';0)\,V_L(r)\phi_l(r) = 0 . \tag{9}$$

This set of coupled differential equations was solved, using the basis set expansion method discussed below and the coordinate rotation method outlined earlier, to generate our quantum state energies and lifetimes.

D. Basis considerations

The eigenfunctions of J^2 and J_z introduced in Eq. (3) as angular basis functions can be simplified in light of the restrictions placed on J and M:

$$\Psi_{j,l}^{J=0,M=0}(\theta,\phi,\theta_0,\phi_0) = N_l\,\delta_{jl}P_l[\cos(\theta)] , \tag{10}$$

where P_l is the lth order Legendre polynomial and N_l is a normalizing constant. Test calculations using this basis set indicated that at least 20 Legendre polynomials had to be included to achieve results which were stable with respect to the inclusion of more (i.e., higher order) polynomials. Since the radial functions $\phi_{jl}^{JM}(r)$ of Eq. (4) also need to be described as linear combinations of approximately 20 basis functions (see below), on the order of 20×20 or 400 terms, would arise in our wave functions. It would be fairly time consuming to diagonalize the resulting 400×400 Hamiltonian matrix for many values of the complex scaling factor η. Therefore, to reduce the size of the angular basis and to simplify the interpretation (i.e., make connection with the bending states of DCN) of the Hamiltonian matrix eigenvectors, the original $\{P_l[\cos(\theta)]\}$ basis functions were contracted to yield a new $\{\chi_{v_2}[\cos(\theta)]\}$ basis as detailed in the Appendix. This contraction, when applied to the matrix representation of the Hamiltonian appearing in Eq. (9), resulted in about a threefold reduction in the size of the matrices involved, with no significant decrease in accuracy for the low-energy vibrational states (low values of v_2). We thus view the $\chi_{v_2}[\cos(\theta)]$ basis as the optimal angular basis functions to use in the calculations on DCN described below.

The radial functions $\phi_{jl}^{JM}(r)$ of Eq. (4) were expanded in terms of evenly spaced radial Gaussian basis functions $\{g_i(r)\}$. This same basis proved to be useful in our earlier work[10,12] on rotational predissociation of atom–diatom van der Waals complexes. We write the expansion as follows (using $J = M = 0$, $j = l$):

$$\phi_{jl}^{JM}(r) \equiv \phi_l(r) = \sum_i C_i^l\,g_i(r) , \tag{11}$$

where

$$g_i(r) = N_i\exp[-\gamma_i(r-r_i)^2] . \tag{12}$$

Here, N_i is a normalization constant, and the γ_i and r_i are the exponents and centers of these Gaussians, respectively. The exponents γ_i were chosen to be identical $(\gamma_i = \gamma_0)$ and the r_i were evenly spaced according to

$$r_i = r_0 + (i-1)\Delta r . \tag{13}$$

To be able to describe vibrational states of DCN with a given radial nodal character (e.g., corresponding to various values of v_1, the D--CN stretching quantum number), γ_0 and Δr must be chosen such that successive Gaussians have significant overlap and are spaced at least as closely as are the nodes in the v_1 direction of the vibrational wave function. Achieving an accurate description of states with energy ~1100 cm^{-1} above dis-

sociation (see Sec. III A) dictates the maximum spacing Δr which is acceptable. In the region of the potential well, whose depth is ~4500 cm^{-1}, these states have ~5600 cm^{-1} of vibrational kinetic energy which corresponds to a local de Broglie wavelength of ~0.5 a.u., which would imply that a 0.25 a.u. (or less) spacing of the basis functions is needed. The optimal choice of γ_0 is not as obvious. If the Gaussian functions are too narrow, they cannot be combined as in Eq. (11) to represent a smoothly varying wave function. Through trial and error, we found that to obtain a good description of the bound vibrational states of DCN, an overlap between neighboring Gaussian functions of about 0.5 was needed; this is achieved when $\gamma_0 = 34.7$. Given γ_0 and Δr, the total number of Gaussian basis functions still needs to be specified to complete the basis description. Previous CR calculations carried out by our research group[10,12] indicated that the radial basis must extend one full asymptotic de Broglie wavelength beyond the point where the potential is essentially zero. The potential described in Sec. III B becomes small for $r \sim 4.0$–4.5 a.u. so we centered the last Gaussian at $r = 6.5$ a.u. We note, though, that if the last basis function is centered at $r = 6.5$ a.u., then states with asymptotic de Broglie wavelengths of ~2.5 a.u. or energies $\lesssim 200$ cm^{-1} above dissociation, may not be well described in the asymptotic region. Finally a choice of r_0, the location of the innermost radial basis function, must be made. The value of r_0 should be chosen such that the potential $V(r_0, \theta)$, is much greater than the energy of the states under study (about 1100 cm^{-1} here) for all values of the angle θ. Test calculations on the bound states indicated that $r_0 = 2.5$ a.u. was a reasonable choice. This completes the specification of the radial basis used in this work.

E. Implementation of the coordinate rotation technique

To proceed with the CR approach, the complex Hamiltonian matrix **H** obtained by using Eq. (11) in Eq. (9), premultiplying by $g_j(r)$ and integrating over r must be constructed. Then the generalized eigenvalue problem

$$\mathbf{H}\mathbf{C} = E\,\mathbf{S}\mathbf{C} \tag{14}$$

must be solved. Here

$$H_{l'i',li} = \int r^2\,dr\, g_{i'}(r)\left\{\left[-\frac{\hbar^2}{2\mu_{D,CN}}\left(\frac{1}{r^2}\frac{d}{dr}\left(r^2\frac{d}{dr}\right) - \frac{l(l+1)}{r^2}\right) + \epsilon_l\right]\delta_{l'l} + \sum_L f_L(ll, l'l'; 0)\,V_L(r)\right\} g_i(r) \tag{15}$$

and

$$S_{l'i',li} = \delta_{l'l}\int r^2\,dr\, g_{i'}(r) g_i(r)\ . \tag{16}$$

This can be rewritten using standard techniques

$$\tilde{\mathbf{H}}\tilde{\mathbf{C}} = E\tilde{\mathbf{C}}\ , \tag{17}$$

where

$$\tilde{\mathbf{H}} = \mathbf{S}^{-1/2}\mathbf{H}\,\mathbf{S}^{-1/2} \tag{18}$$

and

$$\tilde{\mathbf{C}} = \mathbf{S}^{1/2}\mathbf{C}\ . \tag{19}$$

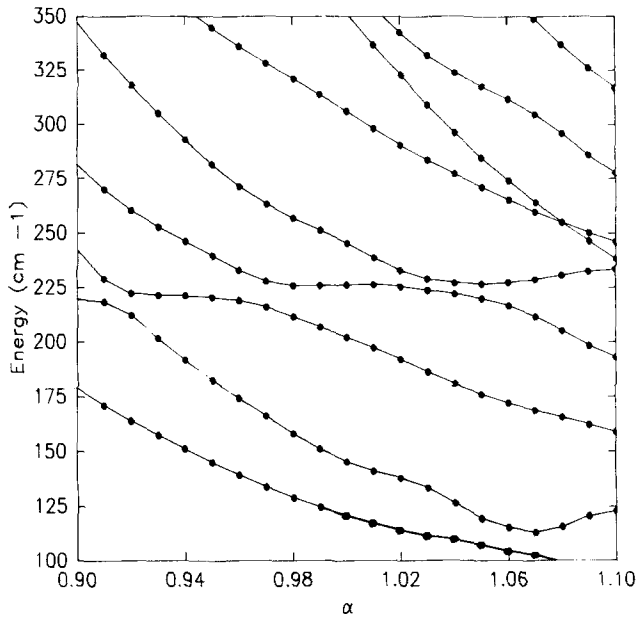

FIG. 3. A typical stabilization plot showing the stabilization resonances at 124 and 225 cm^{-1}.

Since the application of the CR method involves scaling the radial coordinate in the Hamiltonian, the **S** matrix is unaffected; it is a real symmetric matrix whose construction is straightforward. Because it is real valued, its construction need not be repeated as the CR scale parameter η is varied. In contrast, the kinetic energy terms in Eq. (15) must be premultiplied by η^{-2}; the ϵ_l term remains unscaled because it has no r dependence. The η-scaled contributions from the $V_L(r)$ term

$$V^L_{i',i} \equiv \int_{r_{min}}^{\infty} r^2\,dr\, g_{i'}(r) V_L(\eta r) g_i(r) \tag{20}$$

can be reexpressed in terms of integrals over Gaussian functions whose coordinates have been complex scaled,

$$V^L_{i',i} \approx \eta^{-3}\int_{r_{min}}^{\infty} r^2\,dr\, g_{i'}(\eta^{-1}r) V_L(r) g_i(\eta^{-1}r)\ . \tag{21}$$

These integrals must be evaluated [numerically, since $V_L(r)$ is only known in digital form] for every value of η, unlike the other terms in Eq. (15) which require only one numerical integration for a given basis. Though this adds somewhat to the expense of the calculation, the greatest expense is found to be the diagonalization of the Hamiltonian matrix, not its construction.

Another important consideration which arises in the CR approach is locating the optimal scale factor η (i.e., the values of η at which stable behavior is observed in the CR θ trajectories). Since $\eta = \alpha e^{i\theta}$, this gives rise to a two-dimensional search for the α and θ at which a given complex energy is stable with respect to small variations. One search technique which has proven useful for obtaining reasonable estimates of the best α value is the so-called stabilization method[17] in which θ is set to zero and the eigenvalues of $\tilde{H}$ are monitored as α is varied. A typical stabilization plot of these eigenvalues as functions of α is shown in Fig. 3 (only a narrow energy range involving a few of the $\tilde{H}$ eigenvalues is shown). In this approach, one looks for

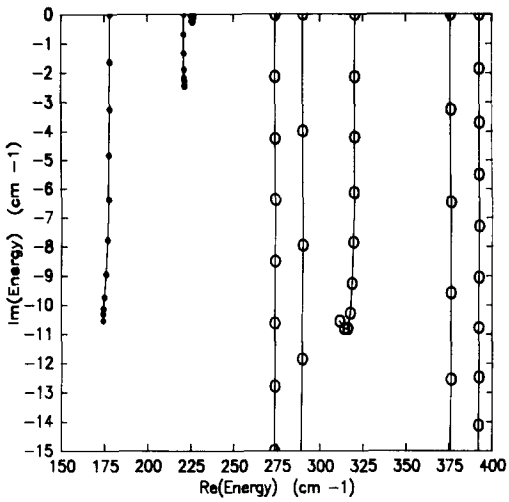

FIG. 4. A typical coordinate rotation θ-trajectory plot at $\alpha = 1.045$ and $0 \le \theta \le 0.004$ rad, the real and imaginary values of the eigenenergies are plotted as points on the graph. By plotting several of these points from different values of θ, resonance behavior is seen when the points start to cluster. Resonance is seen at energies at 175 and 220 cm^{-1} (●). The other eigenenergies (○) do not show signs of resonance since their energy variation with θ $dE/d\theta$ is actually rather constant (N.B., the real and imaginary energy scales are vastly different. This makes the root near 320 cm^{-1} seem to be stable; however, it is not).

avoided crossings between pairs of eigenvalues and uses a value of α near the avoided crossing as a starting value for use in subsequent optimization of the phase (θ) of η.

Given such an initial approximation to the optimal α, θ is varied and the (complex) eigenvalues of $\bar{H}$ are monitored to see whether one or more eigenvalues become relatively insensitive to variations in θ above some critical value of θ (θ_c). If such critical-θ behavior[8] is established, one presumably has located a resonance. In practice, perfect insensitivy to θ is never achieved. Therefore several such θ trajectories (plots of eigenvalues of $\bar{H}$ as θ varies) for nearby α values are usually examined. By plotting these θ trajectories (see Fig. 4), one can usually identify the resonance energies by locating regions of relative insensitivity of the complex energy to variations in both α and θ. The complex energy of the resonance is then taken to lie in this region.

IV. RESULTS OF THE CALCULATIONS

A. Extrapolation of bound-state energies for DCN

Diagonalization of the $\bar{H}$ matrix of Eq. (18) gave rise to 12 (v_1, v_2) energy levels which were bound. The energy spacings of these states were not sufficiently close to those observed by MS to permit straightforward identification (labeling by v_1 and v_2). Hence the eigenfunctions of our bound states (for $\eta = 1$) were plotted as functions of the coordinates r and $\cos\theta$ and their nodal patterns and average radial and angular displacements were examined. By this analysis, reliable assignments of v_1 and v_2 quantum numbers to our energy levels were possible. Our final assignments of the energies of all 12 bound states are shown in Table I.

The energy spacings of our bound states were used to extrapolate into the dissociative region (to ~1100 cm^{-1} above dissociation) to give an idea of which metastable states we should expect to find in the energy range studied. In carrying out this extrapolation, the $v_1 v_2 \rightarrow v_1, v_2 + 1$ energy spacings beyond the dissociation threshold were chosen to be within ~14% of the nearest $v_1, v_2 \rightarrow v_1, v_2 - 1$ spacing and to give $v_1, v_2 \rightarrow v_1 + 1, v_2$ spacings of nearly constant size. This was done to mimic the weak v_2 dependence of the experimental spacings in various v_1 lines. Obviously, the energies thus predicted are very approximate. Nevertheless, assigning a value of v_1 to the metastable states is useful since we expect from our earlier classical dynamics work[7] that increasing the excitation of the v_1 (NC--D stretching) mode can be reasonably expected to correlate with shortening the lifetimes of these states. The resultant estimates shown in Table I indicate that we should be able to locate a number of resonances within ~1100 cm^{-1} of the dissociation threshold and that these states should have v_1, v_2 quantum numbers (and hence lifetimes) which vary substantially.

By examining our bound-state energy differences (shown in Table I), we saw that energy progressions in the v_1 mode [e.g., (0, 0), (1, 0), (2, 0)] exhibited marked anharmonicity. This fact prompted us to repeat our earlier classical trajectory calculations (which ignored v_1 anharmonicity) using more appropriate state energies obtained by including similar anharmonicity in the v_1 mode. The resultant state energies used in these trajectory calculations are referred to as extrapolation

TABLE I. DCN state energies and spacings.

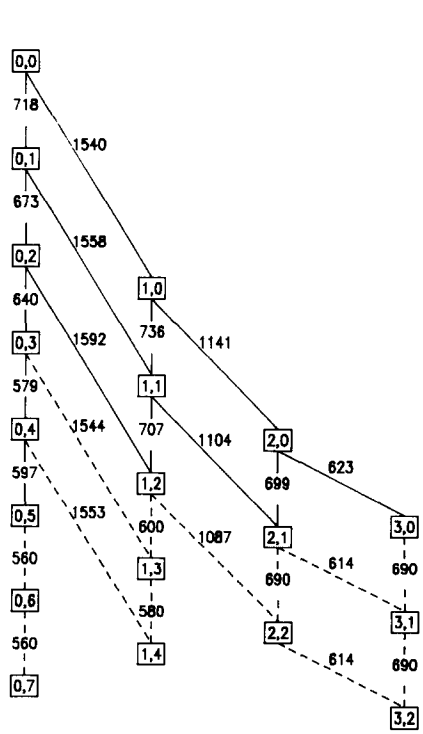

v_1, v_2	Energy, cm^{-1}
0,0	−3579
0,1	−2861
0,2	−2188
1,0	−2039
0,3	−1548
1,1	−1303
0,4	− 969
2,0	− 898
1,2	− 596
0,5	− 372
3,0	− 275
2,1	− 199
1,3	4*
0,6	188*
3,1	415*
2,2	491*
1,4	584*
0,7	748*
3,2	1105*

*extrapolations (See Sec. IV.B.)

TABLE II. Stabilization graph predictions.

v_1, v_2	Energy (cm^{-1})	Optimal α values
1, 3	124	1.06
0, 6	225	0.92, 1.03, 0.98, 1.11
3, 1	390	0.98, 1.04
2, 2	525, 550	1.08, 1.03
1, 4	700	0.98
0, 7	830	0.93
3, 2	1000	0.99 – 1.03

estimates in Table IV. The decay kinetics of these new classical dynamics calculations are summarized in Table V, and comparisons to the corresponding CR results are discussed in detail in Sec. V C.

B. Stabilization and θ-trajectory results

Our stabilization plots indicated that resonances should lie at the energies listed in Table II, where tentative quantum number assignments are also given. Some eigenvalues of $\tilde{H}$ undergo more than one avoided crossing as α is varied (see Fig. 3). Thus in Table II some of the resonance-state candidates can be labeled by more than one optimal α. Most of these stabilization-predicted energies do indeed lie within the energy ranges predicted by extrapolation of the bound-state energies (Table I). The stabilization plots were also used to obtain estimates of the best α values to use in computing CR θ trajectories. These values of α are those given in Table II.

Given the above estimates of the optimal α values corresponding to each resonance state, θ trajectories were carried out for nearby values of α. After examining numerous θ trajectories (e.g., see Fig. 4), a number of candidates for resonances (see Table III) were located, some of which appeared to be stable for more than one value of α, because their stabilization graphs showed avoided-crossing behavior at more than one α value. A totally unambiguous assignment (v_1 and v_2 labeling) of all the roots exhibiting resonance behavior was very difficult partially due to the fact that any finite basis shows imperfect behavior with respect to variations in η. Nevertheless, we feel that the results shown in Table III represent our best effort at identifying the quantum resonance states of DCN which lie within ~1000 cm^{-1} of dissociation.

TABLE III. Coordinate rotation (θ trajectory) assignments.

v_1, v_2	Energy[a] (cm^{-1})	Width[b] (cm^{-1})	α
1,3	175	20	1.045
0,6	220	5	1.045
3,1	385	30	1.06
2,2	505	100	1.04
1,4	608	80	0.96
0,7	716	30	0.97
3,2	890,895	100	0.95, 1.055

[a]The real part of the complex energy eigenvalue.
[b]The width $\Gamma = -2\,\mathrm{Im}$ (complex energy eigenvalue).

V. INTERPRETATION OF RESULTS AND QUANTAL-CLASSICAL COMPARISON

A. Technical differences

At this stage, we stop to recall that technical differences exist which complicate the comparison of the classical and quantal results. We used the $V_L P_L$ fit [Eq. (1)] of the CI-calculated potential energies in the present CR study, whereas our earlier classical analysis used a polynomial fit of the same CI energies. This difference introduces a quantitative (but not qualitative) difference in the potential energy. Second, the *ab initio* CR analysis achieved its own energetic information about the vibrational energy levels of the molecule, whereas the classical analysis required this knowledge as input. So, the CR dynamical behavior is linked unambiguously to its energetic information (e.g., no harmonic or anharmonic extrapolations of the v_1 energies are required). As discussed earlier, we have used all of the concrete information available about the energetics of the DCN vibrational states in order to counteract the variability of the classical method and thereby make the quantal–classical comparison as objective as possible. Lastly, both our classical and quantum mechanical analyses neglect the vibrational contribution of the DC--N bond. Though there is supportive evidence that motion in this mode should not be a major influence, its exclusion affects the comparison of our theoretical results to the experimental interpretation. With these differences in mind, we proceed now to the actual comparison of both energies and lifetimes obtained in our quantal investigations to the classical results and to those inferred from the experimental absorption and PFES spectra.

B. Comparison of metastable-state energies

The extrapolation, stabilization, and CR estimates of the resonance-state energies are shown in Table IV to permit direct comparisons. We see that the stabilization-based energies varied less than 115 cm^{-1} from the CR energies. The resonance energies based upon extrapolation of the bound-state CR energies also differ

TABLE IV. Energies of selected metastable states of DCN (in cm^{-1}).

v_1, v_2	Extrapolated[a]	Stabilization	CR	Experimental[b] ±135
1, 3	4	124	175	−140
0, 6	188	225	220	340
3, 1	415	390	385	•••
2, 2	491	525, 550	505	(660)
1, 4	584	700	608	540
0, 7	748	830	716	1040
3, 2	1105	1000	890, 895	•••

[a]Energies used for classical dynamical study whose results are given in Table V (see Sec. IV A).
[b]Obtained from MS line spacings; the number in parentheses is based on a tentative assignment (see Sec. IV A).

by no more than 120 cm^{-1} from the stabilization-based energies. The fact that the extrapolation and stabilization estimates are remarkably close to the CR values supports the use of these cruder methods to help locate the CR energy levels and to characterize the quantum numbers of those states.

Table IV also shows a list of what we refer to as experimental vibrational state energies. We estimated the zero-point energies and determined subsequent energy increases from MS's interpretation of their absorption spectrum. The uncertainty of 135 cm^{-1} estimated for these energies is partially due to experimental uncertainty in absorption peak positions but mostly due to uncertainty in the dissociation threshold. The state energies corresponding to $v_1=3$ were not available in the MS manuscript and the $v_1=2$ assignment was somewhat tentative (see Sec. I A).

The (1, 3) state is expected to be bound according to the available experimental data. However, all our calculations predicted the (1, 3) state to be unbound and to have a resonance energy at the critically low energy (< 200 cm^{-1}, discussed at the end of Sec. III D), where we expect our radial basis $[g_i(r)]$ to be deficient. Thus, it is likely that CR substantially overestimates the energy of the (1, 3) state. The fact that we predict (1, 3) to be unbound whereas experimentally it is expected to be barely bound is probably a result of our potential surface not being entirely correct in this energy range. There are other noticeable differences between the estimated experimental state energies and our CR energies. All comparisons directly to energies determined from the MS data are within 321 cm^{-1}, which is not always within the estimated uncertainty in the experimentally based numbers. These theoretical–experimental energy differences are not large, however, and may also be attributed to differences incurred in our description of the potential energy surface (see Secs. III B and V A).

C. Comparison of lifetimes

We have listed in Table V the lifetimes calculated by both CR and our earlier classical trajectory method. The lifetime (τ) is defined as the time necessary for the population to decrease to e^{-1} (i.e., $N/N_0=e^{-t/\tau}$). We recall that the state's width (Γ) is inversely proportional to its lifetime ($\Gamma=\hbar/\tau$). The remainder of this discussion will focus on state lifetimes, although analogous comparisons can be made with the widths.

Direct comparison of the CR lifetimes to experimental lifetimes is difficult. MS reported[3] only rough estimates of lifetimes based upon absorption linewidths and polarization retention. Lifetimes of $0.1 \leq \tau \leq 0.7$ ps are consistent with the linewidths $0.4 \geq \Delta\lambda \geq 0.1$ nm of the MS absorption and photofragment excitation spectra (near 143 nm). These lifetimes are certainly qualitatively comparable to the majority of our CR and classical lifetimes reported in Table V, which we now proceed to compare in detail.

The classical lifetimes shown in Table V were determined by fitting the results of an ensemble of trajectories to an exponential decay profile. For $v_1 \geq 1$ we found that we needed to use a double exponential fit because there was strong evidence of two competing decay processes. Excellent fits are achieved in all cases. These two kinetic processes had rates which were distinctly different. We distinguish them here as a fast, short-lived decay channel and a slow, long-lived decay channel. Because the classical decay kinetics required double-exponential fitting, Table V lists the slow-channel lifetime and the percentage of trajectories which decayed via this slow channel. The remaining percentage decayed via the fast channel with a lifetime of 0.007 ps. We observed this fast lifetime to be independent of the specific quantum state (v_1, v_2) and that most of the trajectories in this channel decay before one vibrational period. The percentage of trajectories in the fast channel increases with an increase in v_1; for $v_1=0$ there was no evidence of the presence of this channel.

TABLE V. Lifetimes of selected metastable states of DCN (in ps).

v_1, v_2	CR[a]	Classical[b]	
1, 3	0.26	0.52	(90%)
0, 6	1.0	0.85	(100%)
3, 1	0.18	0.35	(34%)
2, 2	0.053	0.14	(55%)
1, 4	0.066	0.18	(89%)
0, 7	0.18	0.21	(100%)
3, 2	0.053	0.14	(32%)

[a]Calculated by $\tau=\hbar/\Gamma$.
[b]Parentheses give percentage of slow-channel classical trajectories.

To compare the quantal CR and classical lifetimes, we first recall that the CR method identifies resonance energy states which are imbedded in the continuum. The fast classical channel discussed above appears to describe a direct dissociation component whose rate is independent of the quantum state. This part of the classical trajectory results should therefore be considered to be related to a nonresonant direct dissociation mechanism. The fast classical lifetime is much shorter than any of the CR lifetimes. We therefore conclude that the subpopulation of short-lived classical trajectories should not be related to the resonance behavior of the system. It is also important to note, even though the fraction of trajectories in the fast channel is only dependent on v_1, that the slow-channel lifetime is not directly related only to v_2; both quantum numbers play roles in determining the slow-channel classical decay kinetics.

Let us now proceed to a direct comparison of CR and the slow-channel classical lifetimes. For $v_1=0$ only the slow channel is operative and hence a single-exponential decay process appeared in our classical data. As Table V shows, the classical lifetimes for $v_1=0$ differ from the CR lifetimes by no more than a factor of 1.2. For $v_1=1-3$ we also compare in Table V our quantal CR lifetimes to the slow classical lifetimes determined by a double exponential fit of the classical decay kinetics. The slow-channel classical lifetimes do vary from one quantum state to the next and their trend

is exactly the same as displayed in the CR lifetimes. The CR lifetimes are all shorter than the slow-channel classical lifetimes by a factor of 2 to 2.5.

These results tend to suggest that not only do we obtain a reasonable comparison of *ab initio* CR lifetimes with the available experimental values, but we also see a surprising correlation between the quantum mechanical dynamics and the slow-channel component of an independent classical analysis. Certainly the results of these two methods compare more closely than we had anticipated, considering the differences discussed in Sec. V A, and the commonly raised questions about the appropriateness of using classical mechanics on traditionally quantum mechanical systems (see Secs. I C and VI). Recent CR dynamics and classical trajectory calculations performed in our laboratory on the rotational predissociation of triatomic van der Waals molecules have also indicated that lifetimes predicted classically might be within a factor of 2 of the CR lifetimes. Both the van der Waals systems and the present DCN molecule have low reduced masses and internal energies, and de Broglie wavelengths which one would not expect to allow such close classical-quantum agreement.

VI. SUMMARY

Our quantal CR calculations on the predissociation rates of (v_1, v_2) vibronic states of $C\,^1A'$ DCN are consistent with the experimental data on absorption line broadening and fluorescence polarization. The state energies obtained by extrapolating our bound-state energies and via our stabilization calculations support the (v_1, v_2) assignments which we have made in our CR study.

The decay rates obtained in our quantal CR calculations are in reasonable agreement with our classical trajectory simulations and have been useful in providing insight into the interpretation of the classical results. Since the classical trajectory simulations give rise to pairs of competing decay processes, the classical decay kinetics provide lifetimes for both a fast and a slow decay channel. The fast-channel kinetics seem to describe direct decay and have no dynamical features which can be related to the resonance states found in the CR analysis. In short, the fast-channel classical trajectories do not appear to be part of the quantum mechanical resonance states; they describe the background (nonresonant) component in the language of scattering theory. The classical trajectories belonging to the slow channel do undergo $v_2 \rightarrow v_1$ energy transfer over a time scale (see Table V) of 0.14–0.85 ps which is considerably longer than the time needed for a DCN bending vibration (~0.05 ps). The slow-channel classical lifetimes consistently follow the same trend as the CR lifetimes. Therefore, the slow-channel trajectories are considered to contain the resonance information that is also embodied in the quantal CR analysis. So, although the distribution of classical initial conditions was designed to mimic a (v_1, v_2) resonance state of DCN, some of the resulting trajectories appear to better describe a continuum state with the same energy. In a general sense, this indicates that groups of trajectories with the same energy may not relate to the same component of the quantum state involved. An analogous effect was seen in DeLeon and Heller's work[18] on color quantization of bound states in coupled Morse oscillators. They found that they obtained different portions of the true quantum eigenfunction when using trajectories that had the same energy but which were chosen either from within or outside of their (classical) resonance zones. That is, certain initial conditions gave classical trajectories which spanned only a limited region of the available coordinate space and therefore limited the space over which their color quantization method could develop proper phase interference patterns. We speculate that our slow-channel trajectories, which spend reasonably long times in regions of geometry space where the potential of Fig. 1 is nonvanishing, could be used to generate color quantized versions of (v_1, v_2) wave functions. On the other hand, the fast-channel trajectories spend so little time in the region where the potential energy is nonzero that attempts to generate color-quantized wave functions from them could yield only approximations to the asymptotic (large r) components of the wave function. We are currently examining this hypothesis in our laboratory.

The facts that our quantal and classical results seem to agree well with one another and to be consistent with the experimental data is somewhat satisfying. However, it remains a puzzle to us that the classical dynamics simulations perform as well (when compared to our quantal CR predictions as well as experiment). For the vibronic states studied here, the local deBroglie wavelengths in the v_1 mode are all longer than 0.5 a.u. The DCN potential energy surface is certainly not relatively constant over this (0.5 a.u.) distance scale. Therefore, from this point of view we should not have expected a classical treatment of the DCN dynamics to provide such a close representation of the, presumably more correct, quantal (CR) dynamics. Viewed from another perspective, quantum states contain long-time information about the system. Thus, one would expect that classical trajectories which remained in the region of the interaction potential for long times (τ) might be able to describe a quantum state but only within an energy range $\Delta E \sim \hbar/\tau$ and only if phase information were attached to the trajectory. No such phase information was utilized in our work; nevertheless, the classical trajectories worked very well. As mentioned earlier, we are now investigating this puzzle by looking at the color quantized wave functions generated by trajectories belonging to the slow-channel components.

ACKNOWLEDGMENTS

The authors wish to thank the National Science Foundation for their support through Grant No. 8206845 and for support of the Utah DEC 2060 computer facility.

APPENDIX: ANGULAR BASIS CONSTRUCTION

The main objective of contracting the Legendre polynomial basis functions P_l to form the functions $\chi_{v_2}(\theta)$ was to obtain a bending wave function basis set appropriate for a strongly bound molecule. The $P_l[\cos(\theta)]$ functions are acceptable basis functions for an atom

which is only weakly bound to a rigid rotor. The D atom in DCN, however, spends most of its time near the equilibrium angle (157°) and hence to describe even the zero point bending vibrational wave function requires several P_l's.

In line with our assumption of approximate separability of modes, the D--CN bond length was fixed during generation of the χ_{v_2}'s. The locus of points describing the minimum energy $V(r,\theta)$ along r for each θ was characterized. This locus of points, when used to evaluate the potential energy $V(r,\theta)$, generates an effective bending potential function $V(\theta)$ which was then fitted to a power series in $(\theta-\theta_{\min})$. This one-dimensional potential, when combined with the bending kinetic energy at fixed r, gives rise to a one-dimensional Schrödinger equation which was then solved in the basis of Legendre polynomials $P_l[\cos(\theta)]$. The dimension of the Hamiltonian matrix diagonalized was varied from 6 to 26 and the resulting energy level spectra were compared (for stability with respect to adding more P_l's). With $l_{\max}=25$, the lowest several eigenvalues were quite stable.

The eigenvectors $\{a_{v_2}\}$ of the above problem were then used to define the new χ_{v_2} contracted basis functions

$$\chi_{v_2}(\theta)=\sum_{l=0}^{l_{\max}} a_{lv_2}P_l[\cos(\theta)]\ . \tag{A1}$$

The Hamiltonian matrix of the full two-dimensional potential [Eq. (15)] was constructed in the P_l basis and subsequently projected onto the χ_{v_2} basis

$$H_{i'v_2',iv_2}=8\pi^2\sum_{ll'}(-1)^{l+l'}a_{l'v_2}H_{i'l',il}a_{lv_2}\ . \tag{A2a}$$

Similarly,

$$S_{i'v_2',iv_2}=\delta_{v_2v_2'}(8\pi^2)\int r^2\,dr\,g_i(r)g_i(r)\ . \tag{A2b}$$

For each value of l and l', the contributions to all of the $H_{i'v_2',iv_2}$ were calculated, hence the largest matrix stored was of dimension (number of χ_{v_2}'s × number of radial Gaussian functions). Typically approximately 10 χ_{v_2}'s were included (each containing elements of 26 P_l functions) thus decreasing storage needs by about 85% and decreasing diagonalization times by >94%. Test calculations showed that including more χ_{v_2}'s did not appreciably affect the energies of the 12 bound states of the two-dimensional problem, which probably implies that for states with $v_2\leq 7$, one can trust our angular basis set.

As mentioned in Sec. III D, one other advantage of using the functions $\chi_{v_2}[\cos(\theta)]$ as the basis is that it is easier to interpret the eigenvectors of the full problem. This can be useful when the assignment of a resonance is ambiguous; the dominant basis functions in a given resonance wave function indicate whether v_2 should be large or small, whereas directly examining the uncontracted P_l eigenvector is not particularly useful.

[1] G. Herzberg, *Electronic Spectra and Electronic Structure of Polyatomic Molecules* (Van Nostrand, New York, 1966); G. Herzberg and K. K. Innes, J. Phys. **35**, 842 (1957).

[2] G. A. West, Ph.D. thesis, University of Wisconsin, 1975; L. C. Lee, J. Chem. Phys. **72**, 6414 (1980); A. Mele and H. Okabe, *ibid.* **51**, 4798 (1969).

[3] M. T. Macpherson and J. P. Simons, J. Chem. Soc. Faraday Trans. 2 **74**, 1965 (1978).

[4] We are only attempting to address transitions into vibronic states of DCN in which the ν_3 mode remains in its zero-point level. Clearly, freezing the CN bond length is more severe than simply restricting the CN motion to its zero point. However, computational expense prohibits our extension of the *ab initio* potential energy surface employed here to include the CN bond length as a variable. Thus, freezing this bond length is the best we can do in our attempt to simulate the behavior of various (v_1, v_2, at $v_3=0$) levels of DCN.

[5] D. T. Chuljian and J. Simons, J. Am. Chem. Soc. **104**, 645 (1982).

[6] J. W. Downing, J. Čížek, J. Paldus, and J. Michl, Chem. Phys. Lett. **67**, 377 (1979).

[7] D. T. Chuljian, J. Ozment, and J. Simons, Int. J. Quantum Symp. Chem. **16**, 435 (1982).

[8] See, for example, the entire volume, Int. J. Quantum Chem. **14**, 343 (1978).

[9] (a) S. I. Chu, J. Chem. Phys. **72**, 4772 (1980); (b) K-M. Christoffel and J. M. Bowman, J. Chem. Phys. **78**, 3952 (1983); **74**, 5057 (1981); (c) R. M. Hedges and W. P. Reinhardt, *ibid.* **78**, 3964 (1983).

[10] Z. Bacic and J. Simons, Int. J. Quantum Chem. S **14**, 467 (1980).

[11] A. J. F. Siegert, Phys. Rev. **56**, 750 (1939).

[12] Z. Bacic and J. Simons, Inter. J. Quantum Chem. **21**, 727 (1982). J. N. Bardsley and B. R. Junker, J. Phys. B **5**, L178 (1972); A. D. Isaacson, C. W. McCurdy, and W. H. Miller, Chem. Phys. **34**, 311 (1978).

[13] Our review follows the development made in Ref. 10.

[14] G. M. Schwenzer, S. V. O'Neil, H. F. Schaefer III, C. P. Buskin, and C. F. Benden, J. Chem. Phys. **60**, 2787 (1974).

[15] A. R. Edmonds, *Angular Momentum in Quantum Mechanics* (Princeton University, Princeton, New Jersey, 1957).

[16] I. C. Percival and M. J. Seaton, Proc. Cambridge Philos. Soc. **53**, 654 (1957).

[17] H. S. Taylor, Adv. Chem. Phys. **18**, 91 (1970).

[18] N. DeLeon and E. J. Heller, J. Chem. Phys. **78**, 4005 (1983).